Proximity effects on dimensionality and magnetic ordering in Pd/Fe/Pd trialyers

Thomas P. A. Hase,[1] Matthew S. Brewer,[1] Unnar B. Arnalds,[2] Martina Ahlberg,[2] Vassilios Kapaklis,[2] Matts Björck,[2] Laurence Bouchenoire,[3,4] Paul Thompson,[3,4] Daniel Haskel,[5] Yongseong Choi,[5] Jonathan Lang,[5] Cecilia Sánchez-Hanke,[6] and Björgvin Hjörvarsson[2]

[1]*Department of Physics, University of Warwick, Coventry CV4 7AL, United Kingdom*
[2]*Department of Physics and Astronomy, Uppsala University, Box 516, SE-75120, Uppsala, Sweden*
[3]*Department of Physics, University of Liverpool, Liverpool L69 7ZE, United Kingdom*
[4]*XMaS Beamline, European Synchrotron Radiation Facility, Grenoble, France*
[5]*Advanced Photon Source, Argonne National Laboratory, Argonne, Illinois 60439, USA*
[6]*National Synchrotron Light Source, Brookhaven National Laboratory, Upton, New York 11973, USA*

(Received 13 August 2012; revised manuscript received 21 August 2014; published 2 September 2014)

The element-specific magnetization and ordering in trilayers consisting of 0.3–1.4 monolayer (ML) thick Fe layers embedded in Pd(001) has been determined using x-ray resonant magnetic scattering. The proximity to Fe induces a large moment in the Pd which extends ∼2 nm from the interfaces. The magnetization as a function of temperature is found to differ significantly for the Fe and Pd sublattices: The Pd signal resembles the results obtained by magneto-optical techniques with an *apparent* three-dimensional (3D) to two-dimensional (2D) transition in spatial dimensionality for Fe thickness below ∼1 ML. In stark contrast, the Fe data exhibits a 2D behavior. No ferromagnetic signal is obtained from Fe below the 2D percolation limit in Fe coverage (∼0.7 ML), while Pd shows a ferromagnetic response for all samples. The results are attributed to the temperature dependence of the susceptibility of Pd and a profound local anisotropy of submonolayered Fe.

DOI: 10.1103/PhysRevB.90.104403 PACS number(s): 78.70.Ck, 75.70.Cn, 78.20.Ls, 78.67.Pt

I. INTRODUCTION

The Curie temperature T_C is one of the defining parameters of a ferromagnetic material, marking the transition from the ordered ferromagnetic to a disordered paramagnetic state. In general, this ferromagnetic to paramagnetic transition is characterized by power laws which describe the critical behavior of, for instance, the magnetization, close to T_C. For bulk systems these power laws are universal and the value of the critical exponents (for example, β) are determined by the spin (n) dimensionality and spatial (D) dimensions of the magnetic interactions [1]. The spin dimensionality classes are commonly referred to as Ising ($n = 1$), XY($n = 2$) and Heisenberg ($n = 3$). In bulk materials the transition temperature is independent of volume and can be viewed as a measure of the mean exchange interaction which is uniform throughout the material. However, in thin films the volume independence no longer holds as is evidenced by the profound thickness dependence of the ordering temperature. This thickness dependence is a consequence of the different effective interactions within the outermost layers as compared to the bulk like states [2]. The relative contribution of the interfaces can be altered through the choice of the layer thickness, which allows the Curie temperature to be selected from anywhere between zero and the bulk ordering temperature [3,4]. It is not only the ordering temperature that changes with layer thickness. A transition from three-dimensional (3D) to two-dimensional (2D)-like behavior is observed as the layer thickness is reduced below a critical value (d_c), which in turn depends both on the choice of material and its crystalline orientation [3,5,6].

Calculations of the role of boundary effects in a free standing magnetic film shows that the magnetization of the outermost layers to be different to that found in the center of the film [2]. Furthermore, simulations of the temperature dependence of the intralayer magnetic profile shows a strong dependence on the range of the magnetic interactions [7]. As experimental probes determine the volume averaged magnetization, its temperature dependence only yields an effective exponent β^{eff} whose value will depend on the relative strength of the boundary and bulk interactions. Boundary effects become significant in the ultrathin region and/or where the magnetic interactions extend over several nearest neighbors. In the limit that boundary effects are small and the interaction range confined to nearest neighbors the exponents resemble the relevant universality class (i.e., $\beta^{\text{eff}} \sim \beta$). [3,5,6,8] However, when the magnetic interactions are not uniform the scaling laws become inappropriate for determining the spatial or spin dimensionality and β^{eff} can take nonuniversal values that will depend on both the layer thickness as well as other local boundary effects [7].

To date, studies of the magnetic ordering in thin films has concentrated on materials where the interaction between the magnetic layer and the substrate can be ignored. However, in many layered magnetic systems boundary effects cannot be neglected. A clear example is where proximity effects induce magnetic moments at interfaces. This is readily achieved in many nonmagnetic transition metals through indirect exchange coupling to magnetic impurities [9]. The extension of nonuniform magnetization is, therefore, not restricted to within the ferromagnetic layer, but is a more general interfacial phenomenon. In layered heterostructures where the interface acts as a large 2D defect, the induced magnetization can be large and often extends several nanometers from the magnetic layer [10] with the induced moment contributing significantly to the total moment through the increase in the effective magnetic layer thickness. The resulting magnetic system is therefore composed of spatially varying magnetic interactions and likely to display nonuniversal scaling properties.

The magnetization of Pd/Fe/Pd trilayers, in which the Fe layers are in the monolayer range, are dominated by the induced magnetization in Pd [9,11]. This material combination is therefore a good representative example of a system with

extreme interface effects and can be viewed as a model system for addressing the effects of interfacial ferromagnetic proximity on the magnetic ordering. Previous studies of the temperature dependence of the magnetization, determined from measurements using the magneto-optical Kerr effect (MOKE), are consistent with a crossover in the spatial dimensionality (from 2D to 3D) for Fe thicknesses in the range of 0.5–1.0 ML [11]. These results are both unexpected and counterintuitive, as a single monolayer can be viewed as the archetypal 2D structure. The dimensionality crossover in Pd/Fe/Pd trilayers was rationalized by the presence of magnetic proximity effects, effectively increasing the thickness of the magnetic layer through the induced moment in the Pd layers. This interpretation was supported by first-principles calculations [11], but no direct experimental evidence was available on either the range of the induced magnetization or its effect on the magnetic excitations. Experimental verification of the magnetic profile, as well as the element specific changes in the magnetization is therefore of critical importance in understanding the effect of Fe thickness on both the induced interface magnetization profile and the ordering behavior. Here we exploit resonant synchrotron reflectivity to determine the element specific magnetization and explore the underlying causes of the observed changes in the temperature-dependent magnetization. We will show that the apparent dimensional crossover observed from measurements of β^{eff} does *not* reflect a change in the spatial dimensionality, but is, instead, the result of the interplay between the temperature-dependent susceptibility of the Pd and the effective *spin* dimensionality of the Fe layers. These effects are generic in materials with nonuniform magnetic interactions and are important for understanding the interface contribution to the temperature dependence of the magnetization in thin, interacting magnetic layers.

II. EXPERIMENTAL DETAILS

Epitaxial Pd(Fe) samples were grown on MgO(001) substrates using ultrahigh vacuum DC magnetron sputtering as described in Ref. [11]. A 100-monolayer-thick (ML) Pd(001) layer was deposited onto a 10 ML V(001) seed layer before the growth of a thin Fe layer (0.3, 0.5, 0.7, 1.1, and 1.4 ML). This deposition was followed by the growth of a further 10 ML of Pd. The temperature dependence of the magnetization was determined using MOKE in a longitudinal geometry. All samples showed a ferromagnetic response with an isotropic in-plane anisotropy and an ordering temperature which scaled linearly with the amount of Fe. These measurements reveal *effective* critical exponents consistent with an apparent 2D to 3D crossover in the spatial dimensionality of the magnetic phase transition occurring for Fe thicknesses between 0.4 and 0.9 ML, which is in agreement with previous findings [11–13].

The element-specific measurements of the magnetization were obtained using resonant magnetic scattering (XRMS) which has a high reciprocal space resolution allowing for depth-resolved studies through an appropriate choice of energy and scattering configuration [14]. The experiments were performed on beamlines X13A [15] at the National Synchrotron Light Source, XMaS at the European Synchrotron Radiation Facility [16], and 4-ID-D at the Advanced Photon Source [17]. We measured the scattered intensity for left (I^L) and right (I^R) circularly polarized photons for x-ray energies tuned near the L_3 edge of Fe and Pd. Structural information is contained within the sum ($I^L + I^R$), and the magnetic information in the asymmetry ratio AR $= (I^L - I^R)/(I^L + I^R)$. The XRMS signal measured in the geometry used here is sensitive to the in-plane ferromagnetic moment that lies in the scattering plane [18,19].

III. RESULTS AND DISCUSSION

The specular reflectivity (sum) and asymmetry ratio (AR) determined at the Pd L_3 edge from the 0.5 ML Fe sample at 10 K are displayed in Fig. 1. Similar reflectivity data were recorded for all samples at the Pd edge. Simultaneous fitting of the sum and the AR data (Fig. 1), using the GENX code [20,21] yields both the structural and magnetic profiles, with the later shown in the inset of Fig. 1. The magnetic profile is plotted in terms of the magnetic scattering length, $F_m \times r_0$, where F_m is the magnetic scattering factor, a complex number whose magnitude is proportional to the Pd moment per atom μ_B^{Pd}, and r_0 the classical electron radius. As F_m is a fitting parameter in our approach, we can only determine relative changes in Pd magnetization rather than the absolute value of the Pd moment [22]. Similar spectra were obtained for all the samples at 10 K and a more detailed description of these, and the results obtained at the Fe L_3 edge, will be given in Ref. [23]. The fitted layer parameters were in excellent agreement with the nominal structure and the best-ft magnetic profile of the induced Pd moment is shown in the inset of Fig. 1. At this temperature, the induced Pd moment is found to extend about 2 nm from each side of the interface, in line with our previous theoretical analysis [11]. The sharp dip in the center of the profile corresponds to the position of the Fe layer, which, due to the element specific nature of the resonant scattering, does not contribute to the Pd signal. The

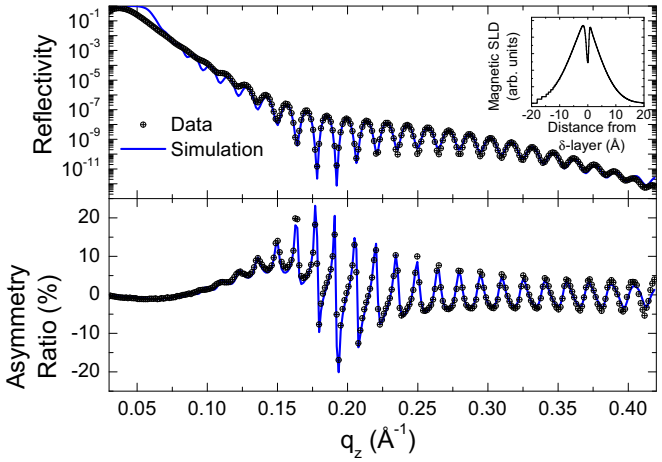

FIG. 1. (Color online) Simultaneously collected structural reflectivity (top) and asymmetry ratio (bottom) from the 0.5 ML Fe sample recorded at the Pd L_3 edge [4-ID-D, APS] (points). Fits (line) are in excellent agreement with nominal growth parameters and show an induced Pd magnetic profile which decays on each side of the Fe interface to a distance of ∼2nm (inset).

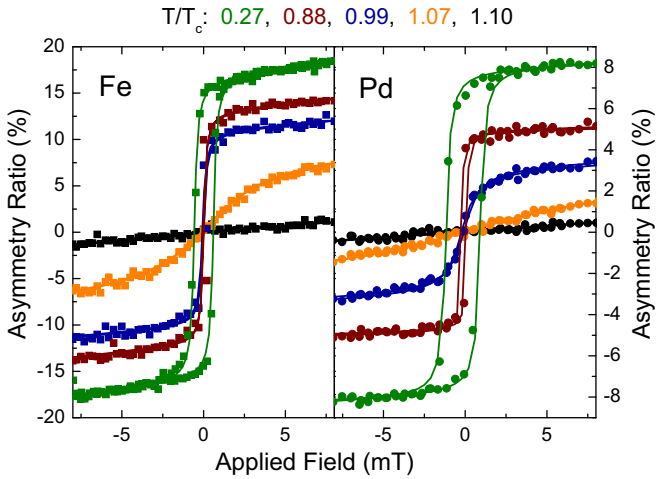

FIG. 2. (Color online) Element-specific hysteresis loops obtained from the 1.4 ML Fe sample at different values of T/T_C. Fe (left) and Pd (right) experimental data (points) are fitted to a pair of arctan functions (line). Both elements show a ferromagnetic to paramagnetic transition at T_C.

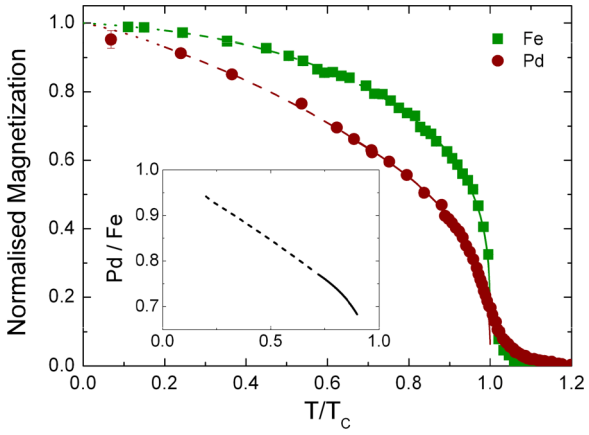

FIG. 3. (Color online) Normalized magnetization of the Fe (squares) and Pd (circles) sublattices for the 1.4 ML Fe sample as a function of T/T_C. The best fit to an effective critical exponent is shown by solid lines with the low temperature behavior parameterized by a polynomial (broken line). Inset: Ratio of the two fitted curves shows a linear dependence with normalized temperature over the range $0.2 \leqslant T/T_C \leqslant 0.8$.

small asymmetry in the magnetization profile, of the order of a few Å, is close to the spatial resolution of the reflectivity probe dictated by the maximum momentum transfer q_{max}. Hence, this asymmetry could be artificial resulting from the limitations of the fitting algorithm. Alternatively, it may be due to different topological roughness on either side of the Fe. However, as the fitted widths of the Pd/Fe and Fe/Pd interfaces are both of the order of 2 Å, the latter explanation is less likely. Any effects due to structural imperfections associated with the Fe deposition on the magnetic profile are effectively averaged spatially by the induced magnetization within the Pd layer. The field dependence of the asymmetry ratio was extracted at a scattering position where the AR was large. This approach yielded element-specific hysteresis loops exemplified in Fig. 2 for the 1.4 ML sample. For this sample, the data recorded at both the Pd and Fe edges exhibit a clear, square ferromagnetic response below T_C. Above T_C, the loops show the classic Langevin paramagnetic shape and the expected collapse of the coercivity to zero.

The hysteresis loops were corrected for the coercive field of the electromagnet and fitted to a pair of arctan functions to facilitate the data reduction. Due to the low coercivity at elevated temperatures, the fitted signal in a field of 0.2 mT was chosen as representative for the spontaneous magnetization. The normalized $[M(T)/M(T=0)]$ temperature dependence of the spontaneous magnetization is displayed in Fig. 3 for the 1.4 ML Fe sample. The larger coercive field observed at the lowest temperature at the Pd edge is an artifact due to the room-temperature correction terms underestimating the reversal of the electromagnet when it was cold, which is exacerbated in the experimental configuration used at the Pd edge. From this hysteresis data it is possible to extract the element specific ordering temperatures, which were, within experimental uncertainties, the same at both edges. The value of T_C was determined as the point on inflection in the normalized temperature dependence that also resulted in the maximum range of linear scaling (Fig. 4). The values of T_C determined using the Pd data as a function of the nominal Fe layer thickness are shown in Table I. The ordering temperature varies linearly with the amount of Fe in agreement with our previous studies. However, the 1.1 ML sample has an ordering temperature that implies an Fe thickness closer to 0.8 ML.

It is also clear from Fig. 3 that the magnetization originating from the Fe and Pd sites are profoundly different: The magnetization of the Pd decreases much more rapidly at low temperatures, while the contribution from Fe appears to be sustained for longer and diminishes more quickly in the vicinity of T_C. These changes can be captured by fitting the results using the relation $M(H = 0.2\,\mathrm{mT}, T) \propto -t^{\beta_{\mathrm{eff}}}$, where $t = T/T_C - 1$. When using a field, albeit small, the signal

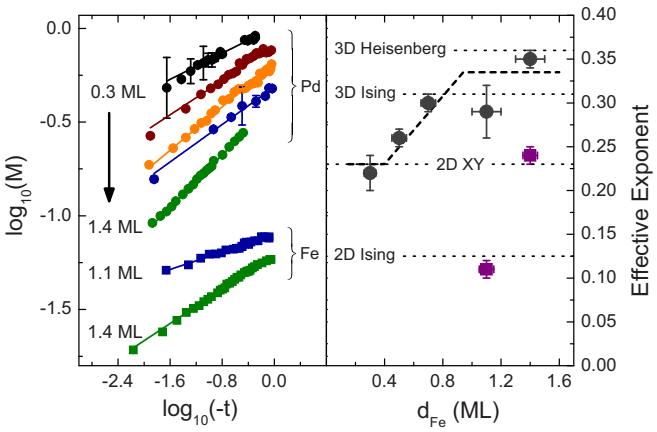

FIG. 4. (Color online) Power-law scaling behavior of the two magnetic sublattices as a function of reduced temperature plotted on base 10 logarithmic axes (left) with data offset for clarity. Effective scaling exponents as a function of nominal Fe thickness (right). The Pd exponents (circles) closely follow the exponents determined using MOKE (broken line). The Fe exponents (squares) could only be measured for samples with an Fe thickness $\geqslant$1 ML.

TABLE I. Ordering temperature (±1 K) determined from the temperature dependence of the remanent magnetization recorded at the Pd L_3 edge.

Nominal Fe thickness (ML)	Ordering temperature (K)
0.3	62
0.5	96
0.7	126
1.1	148
1.4	257

in the immediate vicinity of the transition temperature is affected [3]. The fits to the magnetization were therefore performed over the temperature range 0.5 T_C to 0.98 T_C, capturing the changes in the magnetization of different elemental sites and allowing a direct comparison to the established effective exponents.

As seen in Fig. 4, clear power-law behavior was observed for both the Fe and Pd magnetic sublattices. The temperature dependence of the magnetization of Fe and Pd is remarkably different, as can be seen from both the plotted temperature dependence (Fig. 3) and the obtained effective exponents (Fig. 4). The element-specific exponents of Pd closely track those derived from the previous MOKE analysis [11], especially if the anomalous 1.1 ML sample is replotted with its correct thickness of 0.8 ML, and are consistent with an apparent crossover of the spatial dimensionality of the induced Pd moment occurring for Fe thicknesses in the range 0.4 to 0.9 ML. However, as seen in Fig. 4, β_{eff} for the Fe sublattices differ significantly, reflecting the large differences seen in Fig. 3. As the origin of magnetism in these samples arises from the Fe δ layers, the observation of different temperature dependencies from the two elements runs counter to our simple understanding of strongly interacting sublattices.

To understand these differences, we need to address the interaction between the Fe and Pd layers and the consequences these interactions have on the observed magnetization. The Pd contribution to the magnetization can be obtained using the simple phenomenological model

$$M_{\text{Pd}} \propto \chi_{\text{Pd}}(T) M_{\text{Fe}}, \tag{1}$$

where $\chi_{\text{Pd}}(T)$ is the temperature-dependent susceptibility of Pd and M_{Fe} is the magnetization of Fe. $\chi_{\text{Pd}}(T)$ is therefore proportional to the ratio of the measured $M(T)$ of Pd and Fe and is shown in the inset of Fig. 3. As the electronic structure of elemental Pd is close to the ferromagnetic instability with a Stoner criteria of $S \simeq 9.4$ [24], one would expect that the extent of any induced polarization would be large [25], in line with our experimental observations. $\chi_{\text{Pd}}(T)$ shows a linear dependence with temperature, over the range $0.2 \leqslant T/T_C \leqslant 0.8$, in agreement with bulk measurements [26]. The temperature dependence of the induced Pd moment can therefore be estimated using $M_{\text{Pd}} \propto -\chi_{\text{Pd}}(T) t^{\beta_{\text{eff}}^{\text{Fe}}}$. For the thickest Fe layer, the combination of a linear $\chi(T)$ and a 2D-XY behavior of the Fe results in a magnetization which can easily be mistaken as belonging to one of the 3D classes. A similar effect is observed for the nominal 1.1 ML sample. The measured changes in the magnetization of Pd can be

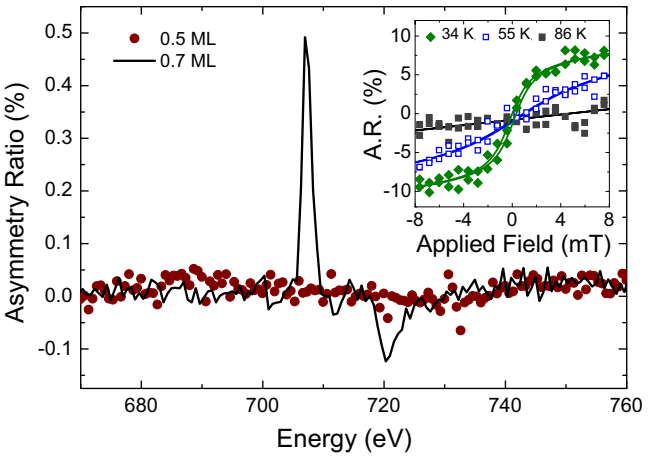

FIG. 5. (Color online) Energy dependence of the asymmetry ratio (AR) determined by reversing the helicity in applied fields of ±8 mT across the Fe L_3 and L_2 edges for the 0.5 (points) and 0.7 ML (line) samples at 30 K. Inset: Field dependence of AR as a function of temperature for the 0.7 ML sample.

reproduced by combining the same $\chi_{\text{Pd}}(T)$ with the measured temperature dependence of the Fe sublattice. The decrease in the effective exponent with decreasing amount of Fe are consistent with an increasing anisotropy within the Fe layer [27], which becomes more pronounced for Fe thickness in the submonolayer range. Similar observations have been made for MLs of Fe on Au [28].

The Pd data, as well as the MOKE results [11], clearly show that all samples possess a long-range ferromagnetic order, with a well-behaved order-disorder transition at T_C. However, a transition temperature was not observed at the Fe edge for all samples. For Fe thicknesses of 0.5 and 0.7 ML the Fe signals no longer resemble that expected from a simple in-plane ferromagnet. The 0.7 ML sample shows a clear resonance at the Fe L_2 and L_3 edges in both the XRMS and magnetic circular dichroism (XMCD) spectra when measured in ±8 mT fields (Fig. 5). However, as shown in the inset of Fig. 5 there is no remanent magnetic signal at any temperature with the hysteresis loops showing a paramagnetic like response with zero coercivity. Furthermore, when the thickness of the Fe layer is 0.5 ML and below, a further change in the Fe behavior was observed: While a clear absorption spectrum (XAS) peak was seen at the Fe $L_{2,3}$ edges no magnetic response was found in the asymmetry ratio or XMCD up to the maximum applied fields that could be obtained (±10 mT).

The lack of magnetic signal from Fe could have two origins: Either the interactions between Fe atoms are favoring a noncollinear ordering, or the susceptibility of possible Fe regions is too low to be affected by the applied field. The paramagnetic like response seen in the 0.7 ML sample favors a noncollinear explanation. One possible noncollinear spin arrangement is a reorientation of the Fe moment to an out-of-plane easy axis, which would not give rise to an XMCD or XRMS signal. Such perpendicular anisotropy (PMA) has been observed in ultrathin, uncapped Pd/Fe bilayers [29], but is normally associated with thicker Fe films grown at low temperature [30,31]. For Pd capped Fe films deposited at 300 K no PMA has been observed and the easy axis remains

confined in the plane [12,32,33]. We thus conclude that PMA is an unlikely source of the noncollinear arrangement and an alternative explanation is required.

When the Fe thickness is below a monolayer the Fe moment is dictated by the local atomic arrangement which could favor an in-plane noncollinear arrangement. Below the percolation limit (∼0.7 ML), the anisotropy of the Fe atoms can be dictated by edge anisotropies, with arbitrary easy axis directions. This anisotropy introduces competing interactions between the randomly placed Fe neighbors [34] (or platelets of Fe) resulting in the Fe atoms behaving as $n = 1$ spins. Thus, the results are consistent with the Fe atoms having a moment, albeit not exhibiting long-range ferromagnetic order. This interpretation requires noncollinear alignment between some of the Fe and Pd atoms, which may be antiferromagnetic (AF) as has been observed in dilute alloys and should, in principle, be verifiable. If the alignment is caused by AF coupling between the elements, Eq. (1) would remain valid and the ordering temperature would scale with the amount of Fe, which is in line with both current and previous findings [11]. The randomly orientated Fe is therefore argued to induce a local moment in the continuous Pd layer, which retains its ferromagnetic order through direct Pd-Pd interactions. In such a case, the resulting temperature dependence of the magnetization of Pd reflects the source magnetization of the Fe which has a strong crystalline anisotropy ($n = 1$), but an unclear spatial dimension. While it is tempting to interpret a value of $\beta^{\text{eff}} \sim 0.23$ as showing $2D - XY$ behavior due to its proximity to the $n = 2, D = 2$ critical value of β, it is important to recall that $\beta^{\text{eff}} \neq \beta$ in this system with strong boundary effects. Thus, although the magnetic excitations existing within the Pd layer are certainly two dimensional, i.e., $D = 2$, it is not appropriate to ascribe any particular value of n to the Pd.

IV. CONCLUSION

The apparent change in spatial dimensionality of the magnetic transition seen in Pd/Fe/Pd trilayers is concluded to be caused by a combination of the temperature dependence of the susceptibility of the Pd layers and the coverage dependence of the local magnetic anisotropy of the ultrathin Fe layers. Due to the large moment carried by the Pd sublattice, nonelement-specific magnetic measurements result in an effective exponent which appears to be 3D above ∼1 ML Fe. Therefore the effective exponents reflect the interplay between the temperature dependence of the Fe-source magnetization and the temperature dependence of the Pd susceptibility $\chi_{\text{Pd}}(T)$. As the Fe thickness decreases the relative importance of the local magnetic anisotropy increases and the spin dimensionality of the Fe is effectively reduced. This gives rise to disordered magnetization within the source layer which has an effective spin dimensionality of 1 (Ising-like).

These results are unexpected, exposing our rudimentary understanding of the nature of proximity-induced magnetization in heterostructures. Boundaries will always give rise to changes in the effective coupling resulting in inhomogeneous magnetization at finite temperatures. Their effects can arise from direct interactions with adjacent materials (as demonstrated herein), be associated with a cutoff in the range of the magnetic interactions [7] or be a complex mixture of the two. To fully capture these effects, which underpin much of current spintronics research, calls for both static and dynamic calculations of the magnetic moments and their interactions to be performed. Currently, there are no analytical solutions available for describing the changes in the induced magnetization with temperature in technologically relevant thin film heterostructures; with results from computational models at fixed temperature only in their infancy [29]. Finally, we have shown that if the spatially integrated induced moment in a material contributes significantly to the total magnetization of a sample, measurements of $M(T)$ may yield exponents for the overall magnetic phase transition that can be misinterpreted. These effects are generic and important for understanding the magnetization in layers which are typically found in many spintronic devices.

ACKNOWLEDGMENTS

The authors acknowledge the financial support of the UK-EPSRC and the Swedish Research Council (VR) as well as the Knut and Alice Wallenberg Foundation (KAW), the Swedish Foundation for International Cooperation in Research and Higher Education (STINT). Work undertaken at the NSLS and the APS were supported by the U.S. DOE, Office of Science, Office of Basic Energy Sciences, under Contracts No. DE-AC02-98CH10886 and No. DE-AC02-06CH11357. XMaS is a midrange facility supported by EPSRC. We are indebted to Simon Brown, Oier Bikondoa, Didier Wermeille, Phil Ryan, David Kearney, and Mike McDowell for invaluable support during beamtime.

[1] J. J. Binney, N. J. Dowrick, A. J. Fisher, and M. E. J. Newman, *The Theory of Critical Phenomena* (Oxford University Press, Oxford, 1993).
[2] K. Binder and P. C. Hohenberg, Phys. Rev. B **9**, 2194 (1974).
[3] F. Huang, M. T. Kief, G. J. Mankey, and R. F. Willis, Phys. Rev. B **49**, 3962 (1994).
[4] X. F. Jin, J. Barthel, J. Shen, S. S. Manoharan, and J. Kirschner, Phys. Rev. B **60**, 11809 (1999).
[5] Y. Li and K. Baberschke, Phys. Rev. Lett. **68**, 1208 (1992).
[6] T. S. Bramfeld, H. Won, and R. F. Willis, J. Appl. Phys. **107**, 09E150 (2010).
[7] A. Taroni and B. Hjörvarsson, Eur. Phys. J. B **77**, 367 (2010).
[8] C. A. Ballentine, R. L. Fink, J. Araya-Pochet, and J. L. Erskine, Phys. Rev. B **41**, 2631 (1990).
[9] A. M. Clogston, B. T. Matthias, M. Peter, H. J. Williams, E. Corenzwit, and R. C. Sherwood, Phys. Rev. **125**, 541 (1962).
[10] J. A. Mydosh, *Spin Glasses: An Experimental Introduction* (Taylor & Francis, London, 1994).

[11] M. Pärnaste, M. Marcellini, E. Holmström, N. Bock, J. Fransson, O. Eriksson, and B. Hjörvarsson, J. Phys.: Condens. Matter **19**, 246213 (2007).
[12] C. Liu and S. D. Bader, Phys. Rev. B **44**, 2205 (1991).
[13] E. Th. Papaioannou, V. Kapaklis, A. Taroni, M. Marcellini, and B. Hjörvarsson, J. Phys.: Condens. Matter **22**, 236004 (2010).
[14] J. M. Tonnerre, L. Sève, D. Raoux, G. Soullié, B. Rodmacq, and P. Wolfers, Phys. Rev. Lett. **75**, 740 (1995).
[15] C. Sánchez-Hanke, C. C. Kao, and S. L. Hulbert, Nucl. Instrum. Methods A **608**, 351 (2009).
[16] S. D. Brown, L. Bouchenoire, D. Bowyer, J. Kervin, D. Laundy, M. J. Longfield, D. Mannix, D. F. Paul, A. Stunault, P. Thompson, M. J. Cooper, C. A. Lucas, and W. G. Stirling, J. Sync. Rad. **8**, 1172 (2001).
[17] J. W. Freeland, J. C. Lang, G. Srajer, R. Winarski, D. Shu, and D. M. Mills, Rev. Sci. Inst. **73**, 1408 (2002).
[18] M. Abes, D. Atkinson, B. K. Tanner, T. R. Charlton, S. Langridge, T. P. A. Hase, M. Ali, C. H. Marrows, B. J. Hickey, A. Neudert, R. J. Hicken, D. Arena, S. B. Wilkins, A. Mirone, and S. Lebegue, Phys. Rev. B **82**, 184412 (2010).
[19] S. D. Brown, L. Bouchenoire, P. Thompson, R. Springell, A. Mirone, W. G. Stirling, A. Beesley, M. F. Thomas, R. C. C. Ward, M. R. Wells, S. Langridge, S. W. Zochowski, and G. H. Lander, Phys. Rev. B **77**, 014427 (2008).
[20] M. Björck and G. Andersson, J. Appl. Crystallogr. **40**, 1174 (2007).
[21] T. P. A. Hase and I. G. Hughes, *Measurements and Their Uncertainties: A Practical Guide to Modern Error Analysis* (Oxford University Press, Oxford, 2010).
[22] M. Björck, M. S. Brewer, U. B. Arnalds, E. Östman, M. Ahlberg, V. Kapaklis, E. Th. Papaioannou, G. Andersson, B. Hjörvarsson, and T. P. A. Hase, J. Surf. Interfac. Mater. **2**, 24 (2014).
[23] M. S. Brewer, U. Arnalds, E. Holmström, G. Andersson, M. Ahlberg, M. Björck, L. Bouchenoire, P. Thompson, D. Haskel, J. Lang, C. J. Kinane, C. Sánchez-Hanke, B. Hjörvarsson, and T. P. A. Hase (unpublished).
[24] T. Herrmannsdörfer, S. Rehmann, W. Wendler, and F. Pobell, J. Low Temp. Phys. **104**, 49 (1996).
[25] H. Chen, N. E. Brener, and J. Callaway, Phys. Rev. B **40**, 1443 (1989).
[26] G. Nieuwenhuys, Adv. Phys. **24**, 515 (1975).
[27] A. Taroni, S. T. Bramwell, and P. C. W. Holdsworth, J. Phys. Condens. Matter **20**, 275233 (2008).
[28] R. Zdyb and E. Bauer, Phys. Rev. Lett. **100**, 155704 (2008).
[29] T. Ueno, M. Sawada, K. Furumoto, T. Tagashira, S. Tohoda, A. Kimura, S. Haraguchi, M. Tsujikawa, T. Oda, H. Namatame, and M. Taniguchi, Phys. Rev. B **85**, 224406 (2012).
[30] X. Le Cann, C. Boeglin, B. Carrière, and K. Hricovini, Phys. Rev. B **54**, 373 (1996).
[31] C. Boeglin, H. Bulou, J. Hommet, X. Le Cann, H. Magnan, P. Le Fèvre, and D. Chandesris, Phys. Rev. B **60**, 4220 (1999).
[32] T. Ueno, M. Nagira, S. Tohoda, T. Tagashira, A. Kimura, M. Sawada, H. Namatame, and M. Taniguchi, e-Journal of Surface Science and Nanotechnology **6**, 246 (2008).
[33] L. Szunyogh, J. Zabloudil, A. Vernes, P. Weinberger, B. Újfalussy, and C. Sommers, Phys. Rev. B **63**, 184408 (2001).
[34] D. J. Webb and J. D. McKinley, Phys. Rev. Lett. **70**, 509 (1993).